Development of thrust stand for low impulse measurement from microthrusters

H. Koizumi
Department of Aeronautics and Astronautics, University of Tokyo, 7-3-1, Hongo, Bunkyo-ku, Tokyo 113-8656, Japan

K. Komurasaki
Department of Advanced Energy, University of Tokyo, 7-3-1, Hongo, Bunkyo-ku, Tokyo 113-8656, Japan

Y. Arakawa
Department of Aeronautics and Astronautics, University of Tokyo, 7-3-1, Hongo, Bunkyo-ku, Tokyo 113-8656, Japan

(Received 17 November 2003; accepted 9 July 2004; published 20 September 2004)

A thrust stand has been developed to accurately measure thrust produced by two types of microthrusters—a liquid propellant pulsed plasma thruster (LP-PPT) and a diode laser ablation microthruster. The impulse of LP-PPT ranged from 20 to 80 μNs. The diode laser microthruster, which is a new type of microthruster, produces much lower impulse range of 1–10 μNs for about 1 s. The mechanical noise induced from the background vibrations becomes a crucial problem for precise estimate of thrust particularly in low impulse measurements. A data analysis method to reduce the effect of mechanical noise is proposed by introducing an additional term in a fitting function. It was verified that the analysis method used in our experimental conditions reduced variance caused by noise down to one-third that of a normal fitting method. The accuracy of the thrust stand is 2.1 μNs in the case of the LP-PPT and 0.7 μNs in the case of the diode laser microthruster. © *2004 American Institute of Physics.* [DOI: 10.1063/1.1790568]

I. INTRODUCTION

Microspacecraft has attracted much attention in recent years because they can potentially reduce launch cost while providing myriad mission capabilities. It is necessary to miniaturize every spacecraft component to achieve microspacecraft production. One component in which a number of researchers are interested is a microthruster,[1] which produces low impulse of 1–100 μNs with an input power of less than 100 W. To date, many kinds of thrusters have been proposed for microspacecraft.

Electric propulsion generates high specific impulse, and can reduce the size and weight of propellant and its tank. However, most electric propulsion systems require a very high power source to function effectively. They are not suitable for microthrusters. Pulsed Plasma Thrusters[2] (PPTs) and Field Emission Electric Propulsions[3] (FEEPs) are considered the only electric propulsion systems that function at low power-levels. There has been renewed interest in them recently.

Impulse measurement is strongly required because a number of microthrusters are repetitively operated in pulses and pulsed thrust is generated. However it is difficult to accurately measure extremely low thrust produced by microthrusters. In the early stage of space development, few studies have addressed low thrust measurement of microthrusters, since the main focus at that time was on developing primary propulsion systems. Stark *et al.*[4] performed a study of low thrust measurement during the early 1970's. They developed a torsional type thrust stand that oscillates horizontally and measured thrust of ion engines ranging from 5 μN to 200 mN. Notwithstanding, that thrust stand was quite complex and expensive. Recently, several studies[5–11] of low thrust measurement using a thrust stand have been done because of the increasing interest in microthrusters. Haag[5] designed a thrust stand with the same mechanism of Stark's, but with simpler components. He measured impulse of (PPT) of 300 μNs. Cubbin *et al.*[6] developed an optical interferometric proximeter for measuring impulse from PPTs within the range of 100 μNs–10 Ns. However, most of microthrusters produce lower impulse (order of 10 μNs) than 100 μNs. Although there are other thrust stands[7–11] allowing measurement of such low thrust, most are specialized for very lightweight thrusters.

In this study a thrust stand has been designed to accurately measure impulse produced by microthrusters. The stand has the same mechanism as Haag's[5] one. In order to estimate the performance, lower impulse (1–80 μNs) was measured and two types of microthrusters: a liquid propellant PPT and a diode laser ablation microthruster were used. The impulses ranged from 20 to 80 μNs and 1–10 μNs, respectively. The mechanical noise induced from the background vibration is a crucial problem for low impulse measurement. A data analysis method to more accurately evaluate such low impulse was established. By adding additional term into a fitting function, actual response from microthruster was separated from mechanical noise. Our method reduced the variance down to one-third that of a normal fitting method.

II. THRUST STAND

A thrust stand addressed here is separated into five components: torsional balance, linear variable differential transducer (LVDT), electromagnetic damper, and flexural pivots. Figure 1 is a schematic diagram of the thrust stand. A thruster is installed on the torsional balance and the counter weight is on the other side. The counter weight allowed the rotating structure to be statically balanced. The rotational axis is supported by two commercially available flexural pivots. That balance swings with the natural period of 4–5 s. Deflection of the balance is detected by the LVDT. An electromagnetic damper is installed to depress undesirable vibrations induced by background vibrations. The damper is turned off before firing a thruster.

Calibration is performed by striking the thrust stand with an impact pendulum. The impact pendulum strikes a force transducer attached on the thrust stand. The force transducer records the history of the impulsive force, whose integral yields the impulse. The impact was varied from 80 to 300 μNs by changing the initial angle of the pendulum. The transducer is 13 cm distant from the rotational axis on the balance; a thruster was from 35 to 45 cm according to the thruster configuration. The effective impulse delivered to the thrust stand was 20–80 μNs.

III. ANALYSIS OF IMPULSE MEASUREMENT

A. Dynamics of a thrust stand

The momentum equation for the torsional balance without damping is

$$\ddot{x} + {\omega_0}^2 x = \frac{l_m l_I}{J} F(t), \tag{1}$$

where l_m is the arm length to the displacement sensor, x is the displacement, and $x/l_m \ll 1$, ω_0 is the natural angular frequency, J is the moment of inertia of the balance about the rotational axis, and $F(t)$ is the applied force to the distance l_I away from the rotational axis. To extend the analysis to the cases for which impulsive force approximation is not valid, the following force with finite pulse width is considered

$$F(t) = \begin{cases} I/t_F & 0 < t \leqslant t_F \\ 0 & t \leqslant 0, t_F < t \end{cases}, \tag{2}$$

where I is the delivered total impulse and t_F is the pulse width of the force. Then the solution for Eq. (1) is

$$x_s(t) = \begin{cases} A\dfrac{1-\cos\,\omega_0 t}{\omega_0 t_F} & 0 < t \leqslant t_F \\ A\dfrac{\sin\,(\omega_0 t_F/2)}{\omega_0 t_F/2}\sin\,\omega_0(t-t_F/2) & t_F < t \end{cases}, \tag{3}$$

where A is the amplitude when $t_F \to 0$,

$$A = \frac{l_l l_m}{J\omega_0} I. \tag{4}$$

The impulse is calculated by measuring this amplitude and comparing it to the result of the calibration.

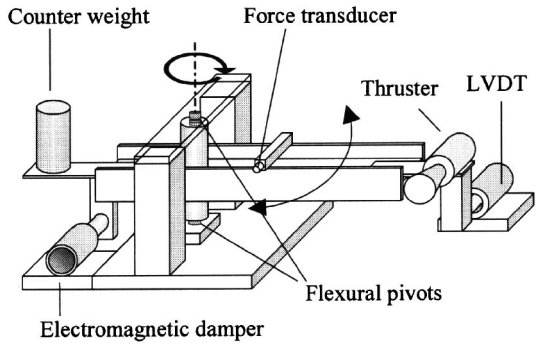

FIG. 1. Schematic diagram of the thrust stand.

B. Analysis method to accurately estimate the amplitude

The constant: A is usually obtained by fitting the ideal thrust stand response $x_s(t)$ on the measured displacement history of the balance. However, such measured data always includes noise. The most serious noise is a mechanical one that is induced on the balance by background vibrations. It includes many components around the natural frequency of the balance that cannot be excluded by a low-pass filter. The associated error becomes serious in case of low impulse measurement or on the condition of large mechanical noise.

Herein, a method separating the actual response of the thrust stand from the mechanical noise is established to accurately measure low impulse. An additional term which expresses the mechanical noise is added in a fitting function. The real mechanical noise includes a number of harmonic components. It is assumed that the noise can be expressed as a sinusoidal wave with the natural frequency because mechanical noise includes a harmonic component of the natural frequency most of all. Let us express the amplitude of the sine component as A_N. Its cosine component is obtained from the position at $t=0$, namely $x(0)$. Then assume a function

$$x_f(t) = x_s(t; A, \omega_0) + A_N \sin(\omega_0 t) + x(0)\cos(\omega_0 t), \tag{5}$$

which is the sum of an ideal thrust stand response and a simulated noise. Constants A and A_N are determined when this function is fitted on measured data. Consequently, the obtained A would include less effect from the noise. The period of this curve-fit should be ranged before the thruster firing to reflect the information of the noise. Hence the curve fit was performed from $-T_0$ to T_0, where T_0 is the natural period of the balance. The Appendix presents discussion of the effect of the fitting period and its optimum value.

C. Verification of analysis methods

Here only the effect of the aforementioned analysis method is shown; the theoretical background is discussed in the Appendix. Noise of the balance was measured during 100 s (the balance was not damped and counterweights were not adjusted). A waveform of 20 s length was arbitrarily extracted from that noise data and superimposed on an ideal impulsive response: a sinusoidal wave with unit amplitude. These artificial data simulate actual data that can be obtained from the thrust stand. More than 200 patterns were prepared by changing the position of extracting the 20 s waveform.

TABLE I. Mean values and variances of obtained amplitudes from two different analysis methods: a normal fitting and a sinusoidal wave with a noise wave.

	Mean Value: μ	Variance: σ^2
Normal fitting	1.0020	0.0306
Fitting with noise	0.9995	0.0124

The signal-to-noise ratio of those data was five, because the standard deviation of the noise was 0.20. Two analysis methods, fitting of a simple sinusoidal wave (normal fitting) and fitting of Eq. (5), were performed for respective artificial data. The original amplitude of the sinusoidal wave was estimated. Table I shows result of the analyses, showing mean values and variances obtained by each method. When Eq. (5) was used as a fitting function, the variance decreased down to one-third and the mean value agreed more with the real value than normal fitting.

IV. VERIFICATION OF IMPULSE MEASUREMENT

A. Liquid propellant pulsed plasma thruster

Pulsed plasma thruster (PPT)[2] is a promising microthruster. Liquid propellant pulsed plasma thruster (LP-PPT)[11,12] is a PPT using liquid propellant instead of solid Teflon® propellant. The thruster is composed of a capacitor, parallel plate electrodes, an ignitor plug, and a liquid propellant injector. High voltage (1.0–3.0 kV) is applied to the electrodes via capacitor (3 μF). The liquid injector injects a few micrograms of liquid propellant (water) into the interelectrode space. The ignitor plug induces are discharged between electrodes to a PPT plasma. The electromagnetic force due to the interaction of the discharge current and self-induced magnetic field accelerates the plasma. The LP-PPT addressed here has been described in the references.[11,12]

In the experiment mechanical noise signals corresponding to a μN thrust were obtained. However they were much less than the impulse level produced by the LP-PPT (100 μNs). The pulsed width of the force was assumed as 0 because the pulsed discharge of the LP-PPT lasted about 10 μs which is much less than the natural period of the thrust stand.

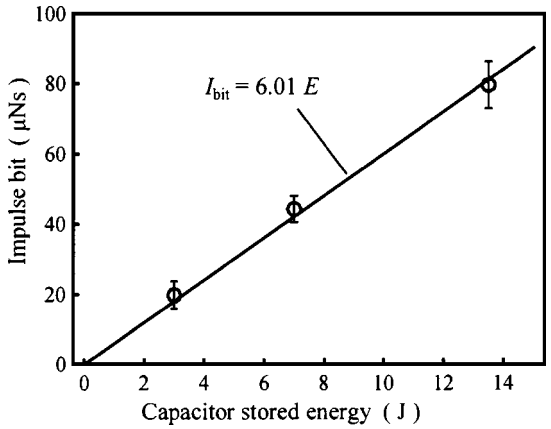

FIG. 2. Dependence of the averaged impulse on capacitor stored energy for liquid propellant pulsed thruster.

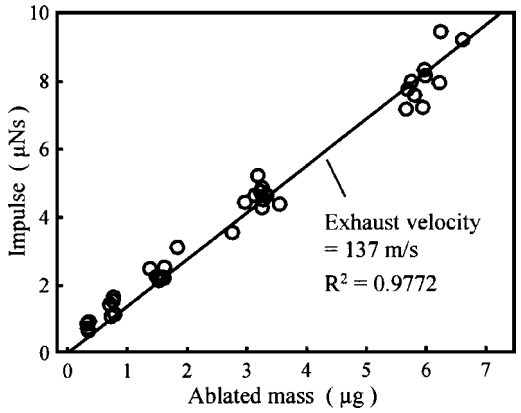

FIG. 3. Dependence of measured impulse on the ablated mass for diode laser ablation microthruster.

Figure 2 shows the dependence of the capacitor-stored energy and the impulse. Every plot of impulse is averaged over more than ten shots; the error bars show the associated standard deviation. The impulse is proportional to the capacitor-stored energy, which is a typical characteristic of PPTs. Also, the shot to shot variation ranged 3.8–6.5 μNs. Those variations are much higher than one caused by the mechanical noise, which were estimated less than 1.0 μNs. Those variations would indicate the shot-to-shot variation of impulse produced by LP-PPT.

B. Diode laser ablation microthruster

A diode laser ablation microthruster[13] produces much lower impulse than PPTs. It comprises a diode laser, an optical system, and target fuel. A laser beam from the diode laser is focused on the target fuel and laser ablation jet is generated to produce thrust. Impulse is variable by changing laser pulse width, since diode lasers are not storage devices but constant power devices.

Impulse produced by the diode laser ablation thruster was measured to verify low impulse measurement of our thrust stand. The thruster addressed in this study was described in the reference.[14] That impulse ranged 0–10 μNs with laser pulse width of 0–800 ms. It was assumed that the thrust was generated at constant force during the laser emission. The analysis method described in Sec. III B was used because the impulse level was comparative with the mechanical noise.

Figure 3 shows the result of measured impulse and the associated ablated mass. Every plot indicates the measured impulse for a single laser pulse shot. The impulse seemed to be proportional to the ablated mass, implying constant exhaust velocity for ablation gas. The measured impulses had some variations from constant exhaust velocity line. Those variations were decreased by the data analysis method described in Sec. III B. In the case of the normal fitting, namely using Eq. (3) as the fitting function, R^2: the coefficient of determination was 0.918. On the other hand, using Eq. (5), R^2 improved to 0.977.

V. DISCUSSION: ERROR ANALYSIS

Error of impulse measurement would be induced by the following causes: noise on the displacement sensor, resolution of a force transducer, resolution of a digital oscilloscope, accuracy of the position of a thruster and force transducer, deviation of angle of the thrust vector, etc.

Noises on the displacement sensor include mechanical noise and other electrical noises. However, only a low frequency mechanical noise induces errors on the curve fitting procedure and the other high frequency noises contribute little (see Appendix). In our experimental conditions, the standard deviation of the mechanical noise was only 1.1 μNs against the thruster impulse of 1–80 μNs. The force transducer resolution was 90 μN from the data sheet. The digital oscilloscope resolution corresponded to 0.4 μNs of impulse. Both positions of the force transducer and the angle of the thrust vector axis of thruster were set within the accuracy of 0.3 mm and 5°, respectively.

First, presume an error caused by a mechanical noise, inducing shot to shot variation when the amplitude of the balance is estimated from displacement data. The accuracy of the amplitude determined by the curve fitting under arbitrary noise is discussed theoretically in the Appendix. According to that result, if normal sinusoidal fitting is performed, the associated error of the amplitude would be 1.0 μNs. In contrast, if fitting function of Eq. (5) is used, this error would be decreased down to 0.6 μNs of impulse.

Second, the accuracy of the calibration constant is addressed. It is given as

$$\alpha = \frac{I_F l_m}{A l_F}, \tag{6}$$

where I_F is impulse measured by the force transducer and l_F is its position from the rotating center of the balance. The uncertainty of the averaged value of I_F over A can be reduced by increasing the number of measurement points. Actually the measurement was performed about 20 times for each condition, and those effects were almost negligible. Uncertainty arose mainly from the error of position measurements of l_m and l_F. Consequently, a typical calibration constant was 49.5 ± 1.2 μNs/V.

The total error of impulse measurement is affected by the errors of both calibration constant and measured amplitude;

$$\Delta I^2 \approx \Delta\alpha^2 A^2 + \Delta A^2 \alpha^2, \tag{7}$$

where ΔA and $\Delta\alpha$ are the uncertainties of the amplitude and calibration constant, respectively. If $\Delta A/A > \Delta\alpha/\alpha$, the amplitude error becomes dominant; thereby, our improved analysis method, curve fit including noise data, would be valid, and vice versa. For instance, for impulse of 1.0 μNs, where the error from the measured amplitude was dominant, the total error would be 1.0 μNs if normal sinusoidal fitting were used. If fitting function Eq. (5) were used, this value would be decreased down to 0.6 μNs. On the other hand, for impulse of 100 μNs, the total error was 2.6 μNs, where the error caused by calibration constant was dominant. Accuracy of positions of the thruster and force transducer becomes particularly important.

APPENDIX: ERROR ASSOCIATED WITH THE SINUSOIDAL CURVE FIT

When an impulsive force is applied to the balance of stationary state, the displacement history of the balance becomes

$$x_s(t) = \begin{cases} 0 & t \leqslant 0 \\ A \sin(\omega_0 t) & t > 0 \end{cases}, \tag{8}$$

which is measured as the signal. the amplitude A is related to the applied impulse by Eq. (4). However, the balance is not actually stationary. Mechanical vibrations and other kinds of noise are included in actual data. The measured signal always includes noise, which causes error of the impulse measurement.

This error is analytically discussed for the case in which the amplitude is determined by the least-squares method. First, let us express an arbitary noise of the period $[-l/2, l/2]$ as the Fourier series,

$$x_N(t) = \sum_{n=1}^{\infty} A_n \sin(\omega_n t + \delta_n), \quad \omega_n = \frac{2n\pi}{l}. \tag{9}$$

Amplitude and phases of its harmonic components are determined from the Fourier series of the noise data. When a fitting function:

$$x_f(t) = \begin{cases} 0 & t \leqslant 0 \\ A_f \sin(\omega_0 t) & t > 0 \end{cases} \tag{10}$$

is fitted on the data with the period $[0, NT_0]$, where N is the arbitary natural number ($n = 1, 2, 3,$ etc.), the squared deviations is

$$\Pi = \int_0^{NT_0} [x_s(t) + x_N(t) - x_f(t)]^2 dt. \tag{11}$$

Differentiating Eq. (11) with respect to A_f and setting it equal to 0 give the amplitude A_f such that the squared-deviations achieves the minimum value. Then the amplitude is obtained as

$$A_f = A + \frac{1}{N} \sum_{n=1}^{\infty} A_n I_n^{(0,NT_0)}, \tag{12}$$

$$I_n^{(T_1 T_2)} = \frac{2}{T_0} \int_{T_1}^{T_2} \sin(\omega_0 t) \sin(\omega_n t + \delta_n) dt, \tag{13}$$

where the first term of Eq. (12) is the actual amplitude and the second term indicates the error caused by the noise Eq. (9). Our interest is in the ensemble averages and variances of the obtained amplitude. Phases of the harmonic components are random within 0 to 2π because the noise is assumed to be a random process. Hence, $\langle \sin(\omega_n t + \delta_n) \rangle = 0$, and $\langle I_n^{(0,NT_0)} \rangle = 0$, where $\langle\ \rangle$ denotes the ensemble average; hence

$$\langle A_f \rangle = A. \tag{14}$$

The mean value determined by the least-squares method agrees with the real value. Next, we calculate the mean square to obtain the variance.

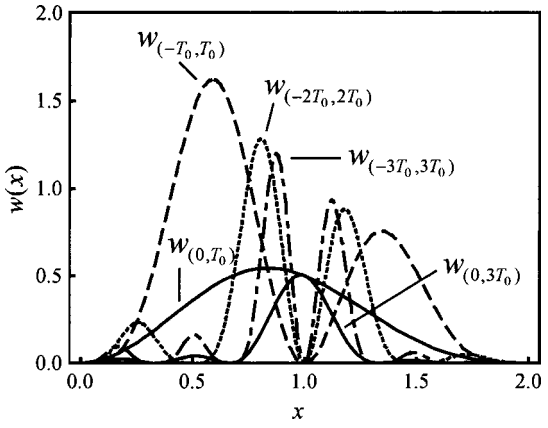

FIG. 4. Weighting functions for the fitting periods: $[0,T_0]$, $[0,2T_0]$, $[-T_0,-T_0]$, $[-2T_0,-2T_0]$, and $[-3T_0,-3T_0]$.

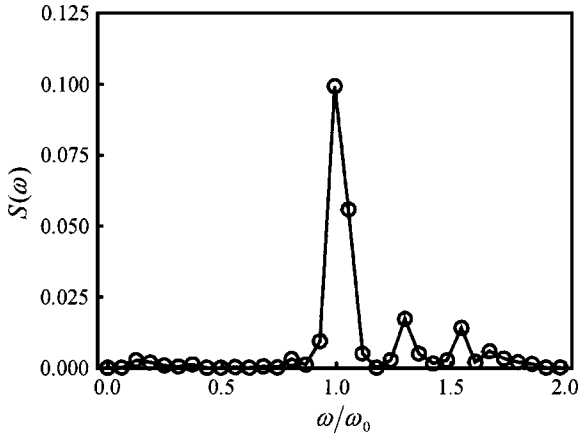

FIG. 5. Power spectrum density of the mechanical noise calculated by FFT from measured displacement of the balance.

$$\langle A_f^2\rangle = A^2 + \sum_{n,m}^{\infty} \langle A_n A_m\rangle \langle I_n^{(0,NT_0)} I_m^{(0,NT_0)}\rangle$$

$$= A^2 + \sum_{n}^{\infty} \langle A_n^2\rangle w_{(0,NT_0)}(\omega_n/\omega_0), \tag{15}$$

$$w_{(0,NT_0)}(x) = \frac{2}{N^2\pi^2}\,\frac{\sin^2(N\pi x)}{(1-x^2)^2}, \tag{16}$$

where $\langle I_n^{(0,NT_0)}\rangle = 0$ and

$$\langle I_n^{(0,NT_0)} I_m^{(0,NT_0)}\rangle = \begin{cases} 0, & n \neq m \\ w_{(0,NT_0)}(\omega_n/\omega_0) & n = m \end{cases} \tag{17}$$

was used. To consider nonperiodic process noise, let $l \to \infty$. Then the summation becomes an integral. Using the relation

$$\lim_{l\to\infty} \frac{l}{4}\langle A_n^2\rangle = 2\pi S(\omega), \tag{18}$$

the means-squared of the amplitude becomes the power spectrum density $S(\omega)$. Hence,

$$\langle A_f^2\rangle = A^2 + 2\int_{-\infty}^{\infty} w_{(0,NT_0)}(\omega/\omega_0) S(\omega)\, d\omega. \tag{19}$$

Finally, we obtained the expression of the variance

$$\sigma^2 = 2\int_{-\infty}^{\infty} w_{(0,NT_0)}(\omega/\omega_0) S(\omega)\, d\omega. \tag{20}$$

Generally the integral of power spectrum of the random process gives its mean-square value of it. The function $w_{(0,NT)}\times(x)$ can be regarded as a weighting function, which is shown in Fig. 4. The weighting function for $N=1$: $w_{(0,NT)}\times(x)$ has a large peak at $x=0.8374$ with width of 0.4 to 1.3. Hence, noise near the natural frequency contributes greatly to the variance. In contrast, the higher frequency component contributes little to the curve fit error because the function decreases biquadratically. The position of the peak shifts toward $x=1$ as the fitting period increases, with touching on the curve of $N=1$; the peak width becomes narrow.

Next, let us consider the case in which a function:

$$x_f^*(t) = \begin{cases} A_N \sin(\omega_0 t) + x(0)\cos(\omega_0 t), & t \leqslant 0 \\ A_f \sin(\omega_0 t) + A_N \sin(\omega_0 t) + x(0)\cos(\omega_0 t), & t > 0, \end{cases} \tag{21}$$

is used as a fitting function and the fitting range is $[-N\,T_0, N\,T_0]$, where N is again an arbitrary natural number. Then the squared deviations is

$$\Pi = \int_{-NT_0}^{NT_0} [x_s(t) + x_N(t) - x_f^*(t)]^2 dt. \tag{22}$$

Amplitude A_f is determined in the same way, as

$$A_f = A + \frac{1}{N}\sum_{n}^{\infty} A_n (I_n^{(0,NT_0)} - I_n^{(-NT_0,0)}). \tag{23}$$

The mean value also agrees with the real value and the variance becomes

$$\sigma^2 = 2\int_{-\infty}^{\infty} w_{(-NT_0,NT_0)}(\omega/\omega_0) S(\omega)\, d\omega, \tag{24}$$

$$w_{(-NT_0,NT_0)}(x) = \frac{8}{N^2\pi^2}\,\frac{\sin^4(N\pi x)}{(1-x^2)^2}. \tag{25}$$

The variance is again expressed as the integral of the power spectrum and a weighting function. The weighting functions for $N=1,2$, and 3 are the shown in Fig. 4. All those functions become zero at $x=1$. Thereby the contribution of the noise of the natural frequency is eliminated. They have two larger peaks on both sides of it than the peak of normal fitting. In general, the mechanical noise has a sharp peak at the natural frequency, and contributions from those side peaks are not serious.

TABLE II. Comparison of the variance: σ^2 of obtained amplitudes from theory and actual curve fit, and its dependence on the fitting period.

Fitting period	Theory	Actual fit
$[0,T_0]$	0.0299	0.0306
$[-T_0,T_0]$	0.0122	0.0124
$[-2T_0,2T_0]$	0.0105	
$[-3T_0,3T_0]$	0.0123	

Figure 5 shows the power spectrum calculated from the measured noise. It has a strong and sharp peak at the natural frequency. The integral of Eq. (24) was calculated for each weighting function using this spectrum. Table II shows the result with variances obtained from the actual fitting of the 210 data. Variances calculated from the theory using Eq. (24) agreed well with variances obtained by fitting Eq. (10) or (21) to the 210 artificial data. Therefore, Eq. (24) was shown to be valid to estimate the variance which would be generated when the amplitude was obtained by the actual curve fit.

Here we conclude that the variance of the amplitude determined by least-squares method can be obtained as the integral of power spectrum density times an appropriate weighting function. Therefore, in order to minimize the associated error, we should measure the power spectrum of the mechanical noise on the balance and then select the best fitting function and period that minimize the integral of Eq. (24). For instance, in our experiment, the optimum fitting method was the fitting functions Eq. (21) and fitting period $[-2T_0, 2T_0]$ which would reduce the variance down to 0.0105 (see Table II).

[1] J. Mueller, *Micropropulsion for Small Spacecraft* (American Institute of Aeronautics and Astronautics, Reston, VA, 2000), Chap. 3.
[2] R. L. Burton and P. J. Turchi, J. Propul. Power **14**, 716 (1998).
[3] S. Marcuccio, A. Genovese, and M. Andrenucci, J. Propul. Power **14**, 774 (1998).
[4] K. W. Stark, T. Dennis, D. McHugh, and T. Williams, NASA Technical Note D-7029, August 1971.
[5] T. W. Haag, Rev. Sci. Instrum. **68**, 2060 (1997).
[6] E. A. Cubbin, J. K. Ziemer, E. Y. Choueiri, and R. G. Jahn, Rev. Sci. Instrum. **68**, 2339 (1997).
[7] M. J. Wilson, S. S. Bushman, and R. L. Burton, 25th International Electric Propulsion Conference, Cleveland, OH, August 24-28 1997, IEPC 97-122.
[8] M. Gamero C. and V. Hruby, 27th International Electric Propulsion Conference, Pasadena, CA, October 15–19, 2001, IEPC-01-235.
[9] A. J. Jamison, A. D. Katsdever, and E. P. Muntz, 27th International Electric Propulsion Conference, Pasadena, CA, October 15–19, 2001, IEPC-01-236.
[10] J. K. Ziemer, 27th International Electric Propulsion Conference, Pasadena, CA, October 15–19, 2001.
[11] H. Koizumi, A. Kakami, Y. Furuta, K. Kimiya, and Y. Arakawa, 28th International Electric Propulsion Conference, Toulouse, France, March 17–21, 2003, IEPC-03-087.
[12] A. Kakami, H. Koizumi, K. Kimiya, and Y. Arakawa, 39th AIAA/ASME/SAE/ASEE Joint Propulsion Conference, Huntsville, AL,20–23 July, 2003.
[13] C. Phipps and J. Luke, AIAA J. **40**, 310 (2002).
[14] H. Koizumi, T. Inoue, K. Kojima, K. Mori, K. Kimiya, and Y. Arakawa, 39th AIAA/ASME/SAE/ASEE Joint Propulsion Conference, Huntsville, AL, 20–23 July, 2003.